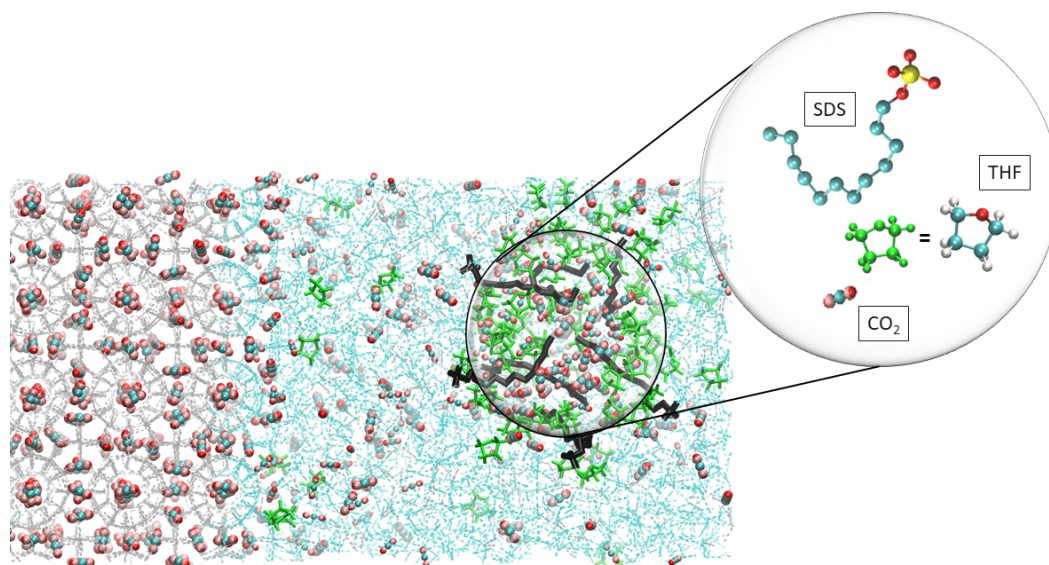


# Graphical Abstract

## Understanding the effect of moderate concentration SDS on CO<sub>2</sub> hydrates growth in the presence of THF

Xinrui Cai, Joshua Worley, Anh Phan, Matteo Salvalaglio, Carolyn Koh, Alberto Striolo



# Highlights

## **Understanding the effect of moderate concentration SDS on CO<sub>2</sub> hydrates growth in the presence of THF**

Xinrui Cai, Joshua Worley, Anh Phan, Matteo Salvalaglio, Carolyn Koh, Alberto Striolo

- SDS and THF promoters are antagonistic when above a temperature threshold
- In the presence of THF and CO<sub>2</sub>, SDS forms micellar aggregates
- Experiments support the simulation insights

# Understanding the effect of moderate concentration SDS on CO<sub>2</sub> hydrates growth in the presence of THF

Xinrui Cai<sup>a</sup>, Joshua Worley<sup>b</sup>, Anh Phan<sup>c</sup>, Matteo Salvalaglio<sup>a</sup>, Carolyn Koh<sup>b</sup>, Alberto Striolo<sup>a,d</sup>

<sup>a</sup>*Thomas Young Centre and Department of Chemical Engineering, University College London, Torrington Place, London, WC1E 7JE, United Kingdom*

<sup>b</sup>*Department of Chemical and Biological Engineering, Colorado School of Mines, Golden, CO 80401, United States*

<sup>c</sup>*School of Chemistry and Chemical Engineering, Faculty of Engineering and Physical Sciences, University of Surrey, Guildford, Surrey GU2 7XH, United Kingdom*

<sup>d</sup>*School of Sustainable Chemical, Biological and Materials Engineering, University of Oklahoma, Norman, OK 73019, United States*

---

## Abstract

### Hypothesis

Additives like Tetrahydrofuran (THF) and Sodium Dodecylsulfate (SDS) improve Carbon Dioxide (CO<sub>2</sub>) hydrates thermal stability and growth rate when used separately. It has been hypothesised that combining them could improve the kinetics of growth and the thermodynamic stability of CO<sub>2</sub> hydrates.

### Simulations and Experiments

We exploit atomistic molecular dynamics simulations to investigate the combined impact of THF and SDS under different temperatures and concentrations. The simulation insights are verified experimentally using pendant drop tensiometry conducted at ambient pressures and high-pressure differential scanning calorimetry.

### Findings

Our simulations revealed that the combination of both additives is synergistic at low temperatures but antagonistic at temperatures above 274.1 K due to the aggregation of SDS molecules induced by THF molecules. These aggregates effectively remove THF and CO<sub>2</sub> from the hydrate-liquid interface, thereby reducing the driving force for hydrates growth. Experiments revealed that the critical micelle concentration of SDS in water decreases by 20% upon the addition of THF. Further experiments in the presence of THF showed that only small amounts of SDS is sufficient to increase the CO<sub>2</sub> storage efficiency by over 40% compared to the results obtained without promoters. These results provide microscopic insights into the mechanisms of THF and SDS promoters on CO<sub>2</sub> hydrates, which allow for determining the optimal conditions for hydrate growth.

*Keywords:* Hydrates, Promoters, CO<sub>2</sub>, SDS, THF

---

## 1. Introduction

- Clathrate hydrates are crystalline compounds. They comprise water molecules that are hydrogen-bonded to each other and guest molecules held by weak Van der Waals

4 forces [1]. There are commonly three types of hydrate structures, namely sI, sII and  
5 sH [2]. sI is the most predominant hydrate structure on earth and contains small  
6 molecules such as CO<sub>2</sub>, and methane [3]. Larger molecules such as Tetrahydrofuran  
7 (THF) occupy larger cages and lead to the formation of sII hydrates instead [4]. These  
8 compounds (sII hydrates) are commonly found under anthropogenic environments [3].

9 Recent studies reported that CO<sub>2</sub> hydrates display great potential in carbon capture  
10 [5], storage [6] and sequestration [7] due to their stability at mild operating condi-  
11 tions at which they can achieve relatively high gas storage [8, 9]. The main obstacles  
12 for these hydrate-based technologies are slow formation rate and low thermal stabil-  
13 ity at ambient conditions [10]. For completeness, it should be pointed out that the  
14 formation of gas hydrates, when undesired and uncontrolled, can lead to negative  
15 consequences. For example, hydrates can cause flow blockage, reducing CO<sub>2</sub> injectiv-  
16 ity during sequestration [11], blocking and sometimes rupturing pipelines and other  
17 equipment [12]. As these occurrences are frequently managed with the use of chemi-  
18 cals, it is important to understand and quantify possible synergistic and antagonistic  
19 effects among various chemicals used in the energy sector.

20 CO<sub>2</sub> hydrate formation, growth and stability can be modulated using chemical addi-  
21 tives. These additives can be classified into thermodynamic and kinetic promoters.  
22 Thermodynamic promoters such as THF and Tetrabutylammonium bromide (TBAB)  
23 shift the melting conditions of hydrates to milder operating conditions (higher tem-  
24 perature and/or lower pressure) [13, 14]. On the other hand, kinetic promoters, usu-  
25 ally surface active materials such as SDS or amino acids, accelerate hydrate growth  
26 [15, 16, 17]. Despite significant research efforts aimed at elucidating the mecha-  
27 nisms responsible for SDS promotion of hydrate growth, a consensus has not yet been  
28 reached. Among the numerous mechanisms proposed are the reduction of interfacial  
29 tension [18, 19] and the capillary effect [20].

30 It has also been observed that SDS alters the surface morphology of hydrates. When  
31 SDS is present, hydrates exhibit upward growth (growth into the gas side) above  
32 the gas-liquid interface. In contrast, in systems without SDS, hydrates tend to grow  
33 downward (growth into the liquid side), which could affect mass transfer phenomena  
34 [21, 22]. Liang et al. observed that lumps of xenon hydrates formed at low SDS  
35 concentrations, whereas a centric layer of hydrates formed at the gas-liquid interface  
36 at high concentrations [22]. They also observed that the gas uptake increases with  
37 increasing SDS concentration, but this upward trend ceased once the critical micelle  
38 concentration (CMC) of SDS was attained.

39 While promoters can enhance the formation and stability of CO<sub>2</sub> hydrates, they can  
40 also have negative impacts. One major drawback is that they may lead to the forma-  
41 tion of mixed hydrates leading to lower CO<sub>2</sub> occupancy since the hydrate cages may  
42 be occupied by the promoters instead. For example, it has been proven experimen-  
43 tally that THF occupies the large cavity of sII cages hence lowering CO<sub>2</sub> gas uptake,  
44 especially when the THF concentration is higher than 5.56% mol [23]. However, Phan  
45 et al. [24] identified a range of temperature and pressure conditions at which CO<sub>2</sub>  
46 hydrates can grow in the presence of small amounts of THF, achieving fast growth  
47 rate without compromising CO<sub>2</sub> storage capacity. Several experiments also reported  
48 an optimal concentration for promoters, and it has been noted that adding more or  
49 fewer promoters reduces their performance [25, 26, 27].

50 Few studies investigated the interactions between thermodynamic and kinetic promot-  
51 ers on hydrate growth. For example, Torre et al. [28] reported that the combination

52 of thermodynamic (THF) and kinetic (SDS) promoters enhances the kinetics of CO<sub>2</sub>  
53 hydrates better than when only a single promoter is used. Veluswamy et al. [15]  
54 also discovered that combining low concentrations of THF and SDS in an unstirred  
55 system dramatically improves the gas uptake of CO<sub>2</sub> hydrates. Yet such synergistic  
56 effect only occurs under specific conditions. For instance, Wang et al. indicated that  
57 2 mol% THF with 0.1 wt% SDS under stirring could improve hydrate formation by  
58 12.7% as compared to the growth in a pure THF solution. However, at a higher  
59 SDS concentration of 0.2 wt%, the improvement drops to 11.7% [29]. The precise  
60 mechanism underlying these observations remains a topic of ongoing debate. Many  
61 argue that the interaction between these two additives and the interface enables the  
62 diffusion of CO<sub>2</sub> molecules [28, 30]. Some attribute the compromised performance at  
63 high concentrations to the formation of SDS micelles [31, 32].

64 In recent years, computer simulations have gained wide popularity as they offer a  
65 cost-effective and efficient way to predict thermodynamic and kinetic properties. By  
66 simulating the complex molecular interactions between water, CO<sub>2</sub> and promoters,  
67 computational simulations provide insights into the fundamental mechanisms that  
68 govern the stability and growth of the hydrates. Furthermore, computational simu-  
69 lations can provide a level of detail that is difficult to achieve through experimental  
70 methods alone. For instance, Phan et al. [24] recently proved, using the direct coexis-  
71 tence method, that THF shifts the equilibrium curve of CO<sub>2</sub> hydrates and facilitates  
72 CO<sub>2</sub> diffusivity into hydrate cages [24]. Several groups also used Monte Carlo simu-  
73 lations to investigate the growth of gas hydrates [33, 34]. These simulation studies  
74 achieved remarkable levels of agreement with experiments while elucidating molecular  
75 phenomena that were previously only hypothesised.

76 Within this landscape, we utilised atomistic MD simulations to understand hydrate  
77 growth in the presence of promoters at the molecular level. By simulating CO<sub>2</sub>  
78 hydrates at different temperatures and promoter concentrations, we aim to decipher  
79 the microscopic mechanism that allows THF and SDS to promote or inhibit hydrate  
80 growth. The remainder of the manuscript is organised as follows: we first introduce  
81 the simulation methodology and report a few details concerning the experimental  
82 techniques used to validate our predictions. We then discuss our results, starting from  
83 the computing simulations and continuing with the experimental validation ones. We  
84 conclude by generalising our results within the context of hydrates application in CO<sub>2</sub>  
85 capture, transport, and storage.

## 86 **2. Methodology**

### 87 *2.1. Methodology*

#### 88 *2.1.1. Simulation Setup*

89 The initial configuration of the simulation box is set up as shown in Figure 1, where  
90 the hydrate phase is sandwiched by the bulk liquid phase along the z-direction. The  
91 hydrate slab, 4.812nm × 4.812nm × 4.812nm in three dimensions, is constructed using  
92 sI CO<sub>2</sub> hydrate cages as it is the most stable structure under our simulation conditions  
93 [35]. The structure of the hydrate cages was built based on the work of Takeuchi [36].  
94 In addition to the 6948 water molecules, 240 CO<sub>2</sub> molecules, 8 SDS molecules and  
95 different amounts of THF (0/50/100) molecules were inserted into the bulk liquid  
96 phase. The concentration of THF in the bulk would thus range from 0mol% to  
97 1.37mol%, which is expected to stabilise hydrates growth [37]. Periodic boundary  
98 conditions are applied in all directions. This renders the hydrate slab infinite in the

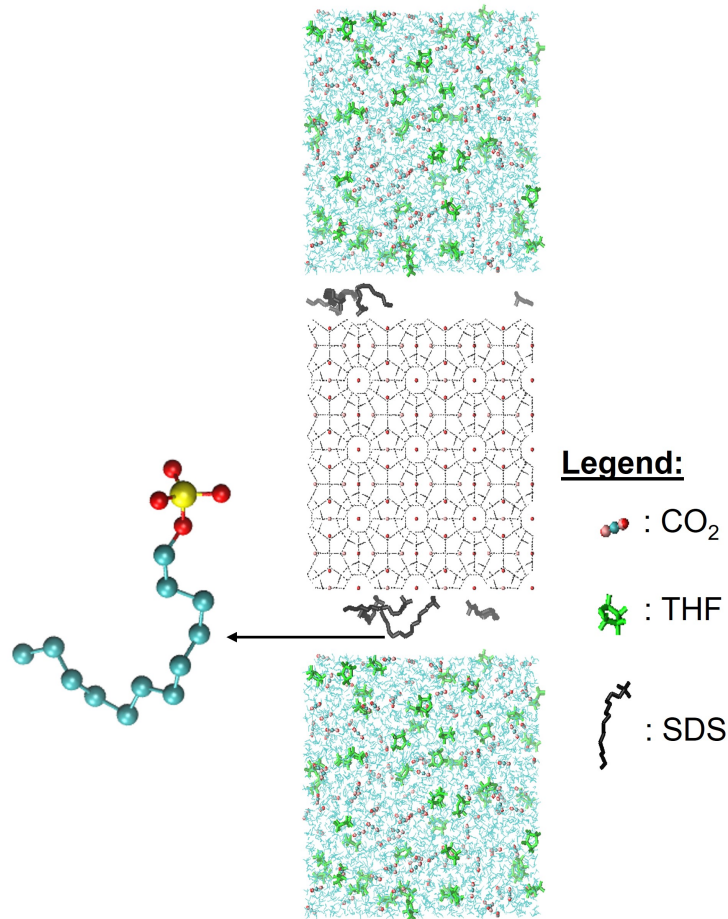


Figure 1: Snapshot of the initial configuration used for simulation. The cyan and grey lines represent water from the hydrate and liquid phases, respectively. Black molecules are SDS, green molecules are THF and cyan and red spheres are carbon and oxygen atoms, respectively, that together form  $\text{CO}_2$ . The chemical structure of SDS is shown on the left, where the cyan, red and yellow spheres represent Carbon, Oxygen and Sulfur atoms, respectively.

99 xy direction, presenting two flat interfaces to the liquid phase perpendicular to the  
 100 z-direction.

### 101 2.1.2. Molecular Models and Force Fields

102 We used the TIP4P/Ice model to describe water molecules as it has been shown that  
 103 this water model reproduces the results that are within a variation of 5K with the  
 104 experimental values [38, 39]. Conde et al. compared the three-phase coexistence  
 105 curve for methane hydrates using TIP4P, TIP4P/2005 and TIP4P/Ice water model  
 106 [40]. The coexistence temperature obtained using the TIP4P/Ice model agrees best  
 107 with experimental results, with only a 5K difference. Miguez et al. also compared  
 108 the three-phase coexistence of  $\text{CO}_2$  hydrates. TIP4P/Ice model predicts a melting  
 109 point only 2K away from the experiment value [39]. The EPM2 [41] force field was  
 110 used to model  $\text{CO}_2$  molecules as several studies have shown its capability to predict  
 111  $\text{CO}_2$  hydrates growth and dissociation [42, 39]. The general AMBER force field [43]  
 112 was used for modelling THF due to its prior success in THF hydrate simulations [24].  
 113 SDS molecules use the TraPPE force field for its hydrocarbon branch [39] and the  
 114 Berkowitz model for the headgroup due to the presence of sulfonate [44]. Non-bonded  
 115 interactions are modelled using electrostatic and dispersion forces. We used Coulomb  
 116 interaction for electrostatic forces with a cut-off at 1.4nm, and the particle mesh Ewald

117 method was chosen for long-range adjustment. Lennard-Jones interactions were also  
118 used for dispersion modelling at a cut-off of 1.4nm. Lorentz-Berthelot combining rules  
119 were used to estimate the LJ interactions for dissimilar atoms.

120 Numerous studies have substantiated the reliability of these forcefields[39, 40, 42]. For  
121 instance, Phan et al. [24] utilised TIP4P/ice, EPM2 and general AMBER forcefields  
122 to simulate CO<sub>2</sub> hydrates. Under these forcefields, the hydrates grow at 269.1K  
123 and 274.1K but initiate dissociation at a temperature of 279.1K. Remarkably, the  
124 dissociation temperature conforms to experimental observations.

### 125 *2.1.3. Algorithm*

126 We employed the direct coexistence method to simulate the growth and dissociation  
127 of CO<sub>2</sub> hydrates where the solid hydrate phase is in direct contact with the bulk liq-  
128 uid phase [45]. We describe the systems with atomistic resolution and integrate the  
129 equations of motion using the software package GROMACS 2021 [46]. The leapfrog  
130 algorithm is used to solve the equation of motion with a 1 fs timestep. Once the  
131 initial configuration is prepared (see Figure 1), our protocol initiates with an energy  
132 minimisation via the steepest decent method. The system is simulated under NPT  
133 condition for 5ns to equilibrate the pressure utilising Berendsen’s pressure coupling  
134 [47] with a time constant of 5 ps. The temperature is controlled using Nosé-Hoover  
135 thermostat with a time constant of 0.5 ps [48]. As shown in Supplementary Informa-  
136 tion (Figure S2), analysis of the simulation results confirms that both the pressure  
137 and the volume of the simulation box converged during the equilibration phase of  
138 our simulations. Finally, 600ns NPT simulation was performed using Nosé-Hoover  
139 thermostat and Parrinello-Rahman barostat [49]. The temperature and pressure were  
140 coupled at a time step of 0.5 ps. This ensures the rapid removal of latent heat released  
141 to the system by the phase transition [50]. By using a semi-isotropic pressure cou-  
142 pling while maintaining the xy interfacial area constant, the system maintained the  
143 pressure normal (z direction) to the hydrate-liquid interface constant. This approach  
144 is commonly implemented to avoid anisotropic pressure distributions due to the fact  
145 that the hydrate substrate is solid, hence its dimensions cannot be changed to main-  
146 tain the desired constant pressure [51]. The melting temperature of CO<sub>2</sub> hydrates at  
147 a pressure of 25.5 bar is experimentally determined to be 279.1K [52]. Our system is  
148 simulated at 269.1K, 274.1K, 279.1K and 284.1K and a pressure of 25.5 bar to favour  
149 hydrate growth. We extracted the configuration at every 50ns interval as the input  
150 and simulated it for a production phase of 1ns used for analysis. The average box  
151 size during the simulation run is 4.812nm, 4.812nm, 14.83 ± 0.15nm in the x, y and  
152 z directions respectively.

### 153 *2.1.4. Thickness Analysis*

154 The growth and dissociation of the hydrate slab are calculated by quantifying its  
155 thickness as a function of simulation time. Whether water molecules are organised  
156 within the crystalline hydrate or are instead disordered in a liquid film is determined  
157 by quantifying the F4 order parameter using equation 1 [53] at every 50 ns

$$F4 = \frac{1}{k} \sum_1^k \cos 3\phi \quad (1)$$

158 In equation 1,  $\phi$  refers to the H-O ... O-H torsional angle and k refers to the num-  
159 ber of H-O...O-H bond pairs with bond length < 0.35nm. The F4 value for water

160 molecules embedded in a hydrate environment is approximately 0.7, while that for  
161 water molecules in the liquid phase is close to 0 [54, 55]. This difference allows us  
162 to distinguish between hydrate and liquid phases, as illustrated in Figure S5 in sup-  
163 porting materials. The region between the bulk liquid and hydrate is the interfacial  
164 transition region where partial hydrate cages are formed. The hydrate thickness is  
165 attained by measuring the width of the region when  $F4 > 0.3$ . The  $F4$  value is com-  
166 puted from 1 ns simulations initiated from structures extracted at 50 ns intervals.  
167 Each of the 1 ns simulations is repeated 5 times by running MD simulations in series  
168 with the same initial configuration to attain an error bar associated with hydrate  
169 thickness. In the Supporting information (Figure S4) we provide a representative  
170 set of simulation results in which prominent changes in system size appear to have  
171 minimal impact on the growth or dissociation of hydrates.

#### 172 *2.1.5. Clustering Analysis*

173 An algorithm was implemented using PLUMED to identify and analyse the largest  
174 cluster of SDS molecules in solution. To this aim, we exploit the contact matrix to  
175 define a graph of connected SDS molecules and then determine the largest SDS cluster  
176 as the largest connected component of the graph [56, 57]. This is done by computing  
177 the distance between the centre of mass of each SDS molecule and defining them  
178 as bonded when the distance between their centres of mass is  $< 0.8\text{nm}$ . Once the  
179 molecules belonging to the largest cluster are identified, we compute the centre of  
180 mass of the cluster and its diameter.  $\text{CO}_2$  and THF molecules are considered trapped  
181 in the SDS cluster when found within the identified cluster radius. This procedure  
182 allows us to obtain aggregate size, aggregation number, and composition within an  
183 aggregate.

#### 184 *2.1.6. Experimental - Pendant Drop Tensiometry*

185 An ambient condition pendant drop tensiometer (KSV instruments) was utilised to  
186 determine the CMC of SDS and SDS-THF solutions. A sketch of the experimental set-  
187 up is presented in Figure S6.  $\text{CO}_2$  saturated de-ionised (DI) water was first prepared  
188 by bubbling  $\text{CO}_2$  through a beaker of DI water for 12 hours. SDS solutions were then  
189 prepared from 0.001M to 0.015M by dissolving SDS into the  $\text{CO}_2$  saturated water.  
190 These solutions were allowed 24 hours to reach equilibrium. The entire series was  
191 tested via the pendant drop technique with the drop suspended in an open cuvette and  
192 monitored for 5 mins for each concentration tested. A total of 3 drops were tested for  
193 each concentration to produce an average surface tension value. The surface tension  
194 (ST) of each solution was calculated by solving the Young-Laplace equations for each  
195 droplet and plotted against the log of concentration to determine the switchover from  
196 the concentration-dependent ST region to the concentration-independent region. A  
197 similar methodology is used to obtain the ST of SDS in a SDS-THF- $\text{CO}_2$  solution.  
198 0.476M of THF was added to SDS solutions ranging from 0.001M to 0.038M SDS,  
199 and ST was tested after a 5 min equilibration period which would minimise THF  
200 evaporation but still allow equilibrium to be reached.

#### 201 *2.1.7. Experimental - High-Pressure Differential Scanning Calorimetry (HP-DSC)*

202 A high pressure and low temperature Differential Scanning Calorimetry (HP-DSC)  
203 apparatus (Setaram microDSC VIIa) was utilised for hydrate growth testing as illus-  
204 trated in Figure S7. Pure  $\text{CO}_2$  hydrates and  $\text{CO}_2$  hydrates formed with a combination  
205 of THF + SDS were examined to determine the effect of the combination of promoters  
206 on hydrate growth and  $\text{CO}_2$  uptake.



207 For the pure CO<sub>2</sub> hydrate experiments, approximately 15mg of DI water was added  
 208 to the DSC cell, which was then sealed and placed into the apparatus. The cell was  
 209 pressurized to 25.5 bar using CO<sub>2</sub> gas (99.998%, General Air). The sample was cooled  
 210 to 253.15K and then heated to 293.15K at a rate of 1K/min for the first cycle to form  
 211 ice and hydrate and induce the memory effect, then three repeat experiments were  
 212 performed with the same limits and a cooling rate of 0.2K/min to allow measurement  
 213 of heat release during dissociation.

214 For the CO<sub>2</sub>-SDS tests, the same procedure was followed except that 0.001M and  
 215 0.038M solutions of SDS (>99.0%, Sigma Aldrich) in DI water were loaded into  
 216 the cell. For the tests that involved the usage of THF, 10wt% solutions of THF  
 217 (>99.9%, Sigma Aldrich) and DI water were loaded into the cell along with different  
 218 concentrations of SDS solutions if needed. In these THF-related tests, the lower  
 219 temperature limit was also increased to 263.15K to maintain the same subcooling as  
 220 for the CO<sub>2</sub> and CO<sub>2</sub>-SDS tests. All other parameters were the same. Conversions  
 221 for CO<sub>2</sub> containing hydrates from each test were calculated in the same manner as  
 222 [58] utilising the constants in Table 1.

-	Heat of Formation (kJ/mol)	Hydration Number	Reference
CO <sub>2</sub> Hydrate	70.8	5.9	[37, 59]
CO <sub>2</sub> -10wt% THF	126.2 <sup>1</sup>	20	[37, 60]

Table 1: Heat of formation and hydration number for CO<sub>2</sub> and CO<sub>2</sub>-THF hydrate

223 For these conversion calculations, all hydrates containing THF and CO<sub>2</sub> were assumed  
 224 to have a heat of dissociation similar to the 10wt% THF system. In cases where mul-  
 225 tiple peaks were discerned, the peaks were first identified and separated by the onset  
 226 temperature and peak maximum temperature to determine which phase was likely  
 227 present (CO<sub>2</sub> or CO<sub>2</sub>-THF hydrate) and utilise the heat of dissociation corresponding  
 228 to that phase. Subsequently, the conversion was computed for each isolated peak, and  
 229 the resulting values were summed up to determine the overall total conversion.

### 230 3. Results and Discussions

#### 231 3.1. Simulated Hydrate Growth/Dissociation

232 Figure 2 presents the simulation results obtained for the hydrate growth profiles at  
 233 all temperatures and THF concentrations considered. The trend line for the growth  
 234 profile is computed using logistic regression via Python’s sklearn linear regression  
 235 library. As seen in Figure 2, the hydrates grow or dissociate quickly within the initial  
 236 100ns and reach a plateau after that. This is due to the change in the composition  
 237 of CO<sub>2</sub> in the bulk liquid, which alters the concentration driving force for hydrates  
 238 growth/dissociation.

239 From the analysis of the growth profile, we observed that hydrates grow when  $T <$   
 240 279.1 K. The melting temperature for systems without a thermodynamic promoter  
 241 (THF) can be inferred as 279.1K, as the hydrate thickness stays roughly constant  
 242 during our simulations at this temperature. This agrees well with experimental re-  
 243 sults where the melting temperature is determined to be around 279.1K [52]. For the

---

<sup>1</sup>There is a wide spread in heat of formation predictions for THF-CO<sub>2</sub> hydrates. This value was selected as it was calculated at nearly identical conditions to the present studies

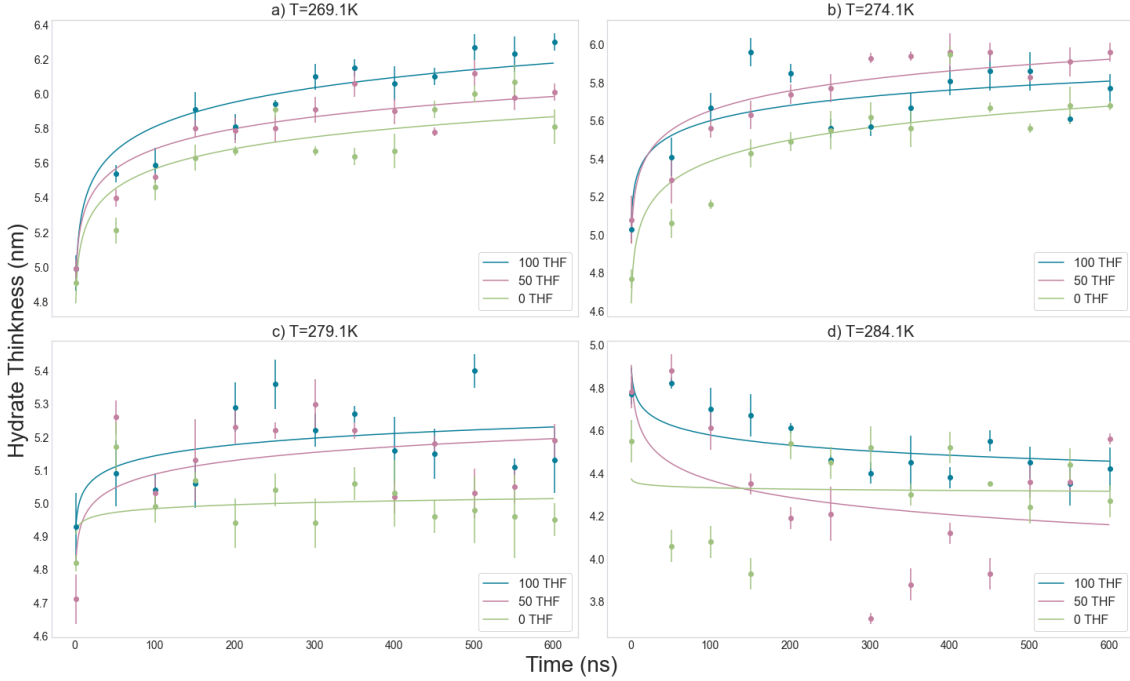


Figure 2: Comparison of hydrate thickness evolution over time with 0/50/100 THF molecules in the system at a)  $T=269.1\text{K}$ , b)  $T=274.1\text{K}$ , c)  $T=279.1\text{K}$  and d)  $T=284.1\text{K}$ . The error bars at 0ns represent the variations of hydrate thickness from 0ns to 1ns.

244 systems with THF present at  $T = 279.1\text{K}$ , there is a minor growth at the beginning,  
 245 but the thickness soon reaches a plateau. The plateau could be due to the reduction  
 246 in driving force as  $\text{CO}_2$  hydrates are formed or the formation of micelle-like aggregates  
 247 that will be discussed further in section 3.3. Above  $279.1\text{K}$ , our results show signs  
 248 of hydrate dissociation, which conforms with the experiments [61, 52]. Noticeably,  
 249 the logistic regression fits the growth profile well at low temperatures. As tempera-  
 250 ture increases beyond  $279.1\text{K}$ , the hydrate growth becomes unstable, and the logistic  
 251 regression model underfits the simulation data, especially when no THF is present.  
 252 This behaviour is expected, as the experiments have shown that the hydrate structure  
 253 fluctuates between dissociation and formation at moderately high temperatures [62].  
 254 In this study, we focus on hydrate growth at low temperatures, where logistic regres-  
 255 sion is effective in describing hydrate growth. We first discuss the results obtained in  
 256 the presence of SDS.

### 257 3.2. Aggregate Formation

258 Visual analysis of the simulation trajectories reveals that the SDS molecules aggregate  
 259 at high temperatures ( $T \geq 274.1\text{K}$ ). To further analyse the aggregation content, we  
 260 plot the component concentration profiles at the end of each simulation, i.e. at 600  
 261 ns.

262 There is no discernible concentration peak at  $T=269.1\text{K}$  as illustrated in Figure 3 (a),  
 263 which reinforced that no aggregation occurred at this temperature. The lines from  
 264 Figure 3 (b) are translated to the right along the x-axis by  $0.25\text{nm}$  for a clearer identi-  
 265 fication of the aggregation cluster. In Figure 3 (b), (c) and (d), the SDS concentration  
 266 peaks shown in the bulk liquid phase indicate the position of the aggregation. The  
 267 alignment of THF and  $\text{CO}_2$  concentration peaks with the SDS aggregation indicates  
 268 that the aggregation also contains  $\text{CO}_2$  and THF molecules. This is confirmed by vi-  
 269 sual analysis of the simulation snapshots. There is also a significant reduction of  $\text{H}_2\text{O}$

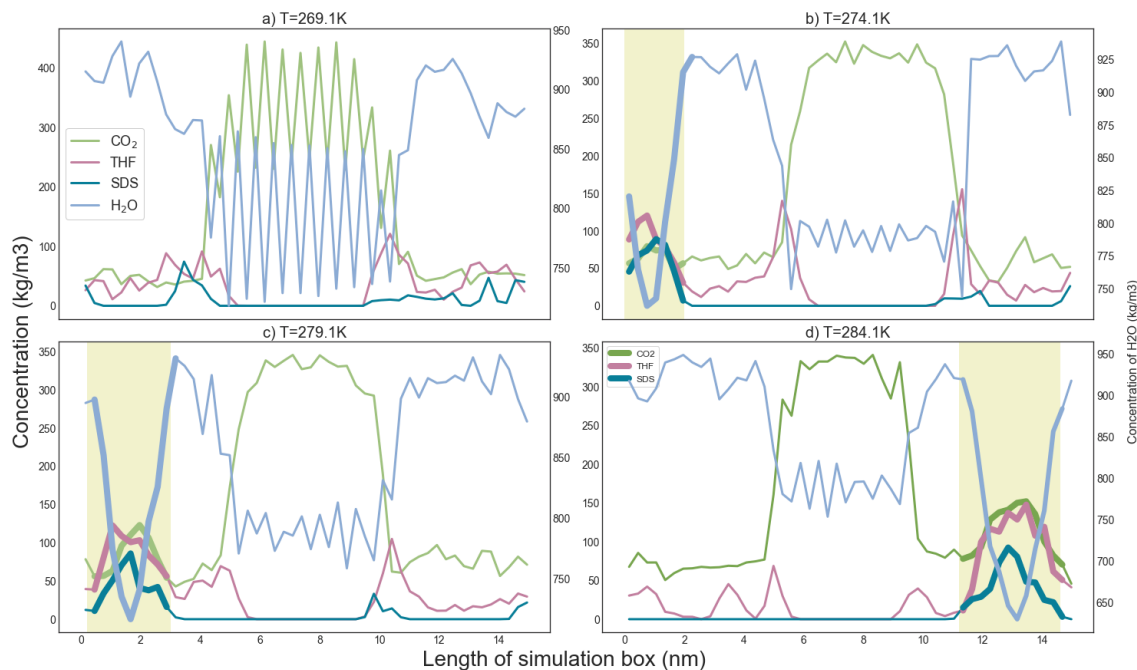


Figure 3: Concentration profiles of CO<sub>2</sub>, THF and SDS molecules within the simulation box with 100 THF molecules at a) T=269.1K, b)T=274.1K, c)T=279.1K, d)T=284.1K. The highlighted regions indicate the position of the aggregate containing SDS, THF and CO<sub>2</sub>.

270 within the aggregates, which indicates that a hydrophobic environment would have  
 271 formed. A closer look at the simulation snapshots using the software VMD (Figure  
 272 4) confirmed that the SDS hydrophobic tails always point towards the centre of the  
 273 aggregates. In contrast, the hydrophilic head groups face towards the aqueous phase.  
 274 Such characteristics suggest that the SDS molecules within the system have indeed  
 275 formed a micelle-like structure.

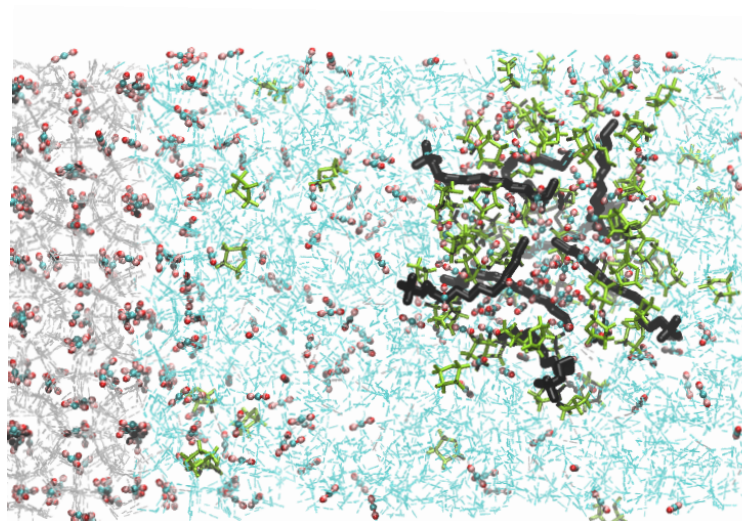


Figure 4: Snapshot of SDS aggregates at T = 284.1K where the black molecules are SDS molecules.

276 Such aggregates are roughly spherical in shape, which is typical of an SDS micelle  
 277 in water at low concentrations [63]. However, SDS micelles in water at ambient  
 278 conditions are usually between 3.5 to 4 nm in size, which is larger than the aggregate  
 279 obtained within our system, which is only 2.5 nm. Additional simulations have been  
 280 performed and it can be seen in Figure S3 that a bigger simulation box would result

281 in a larger SDS aggregate but the increase is very minimal. Such minor differences  
 282 also have insignificant impact on the overall thickness of the hydrate as seen in Figure  
 283 S4.

284 To understand why SDS aggregates in the simulated system yield structures that  
 285 differ from the micelles typically observed in liquid water, we conducted a systematic  
 286 study in which temperature and composition were changed.

Temperature	0 THF	50 THF	100 THF
269.1K	No micelle	No micelle	No micelle
274.1K	No micelle	No micelle	Micelle
279.1K	No micelle	Micelle	Micelle
284.1K	No micelle	Micelle	Micelle

Table 2: Summary of SDS aggregates formation under different temperatures and THF concentrations

287 As seen in Table 2, we did not observe any aggregation in the systems with no  
 288 THF, even at the highest temperature considered. The aggregate phase transition  
 289 temperature increased when the number of THF molecules added to the system was  
 290 halved. Such observation implies that THF reduces the CMC of SDS. The potential  
 291 reason for this phenomenon is that THF may become more insoluble as temperature  
 292 increases due to the closed-loop miscibility gap within the THF-water binary system  
 293 [64]. As such, the insolubility of THF in water at the simulation temperature creates  
 294 an entropic driving force that induces the formation of micelle-like aggregates [65].  
 295 Prior studies also established that the CMC of SDS surfactants decreases linearly  
 296 with a higher concentration of ethers [66], further reinforcing our hypothesis.

297 Figure S8 shows the number of THF molecules trapped within the SDS aggregates  
 298 over the entire trajectory at 274.1K (smallest aggregate) and 284.1K (largest ag-  
 299 gregate). The results are obtained using the clustering algorithm described in the  
 300 Methods section. The number of molecules adsorbed increases initially and reaches  
 301 a constant value when the aggregate is saturated, which is in line with typical mi-  
 302 cellar behaviour. Noticeably, the aggregates trapped more THF molecules at higher  
 303 temperatures.

304 At a similar pressure and concentration used in our set-up, THF will become insoluble  
 305 between  $T = 368 \text{ K}$  to  $404 \text{ K}$  [67], which is warmer than the temperature within our  
 306 system. However, the miscibility behaviour of THF in water is highly sensitive to the  
 307 contamination, and the presence of  $\text{CO}_2$  and SDS may alter the miscibility curve[64].

### 308 3.3. Aggregates Effects on Hydrates Growth

309 The effect of the SDS aggregates on the growth of hydrates can be deduced from  
 310 Figure 2. At  $T=269.1\text{K}$  (Figure 2(a)), where no SDS aggregate is formed in any  
 311 of the three systems, the hydrates have a higher growth rate with increasing THF  
 312 concentration. Similar phenomena are also observed at  $T=279.1\text{K}$  (Figure 2(c)) ,  
 313 where systems with THF form SDS aggregates and agree well with previous studies  
 314 by Phan et al. [24]. However, at  $T=274.1\text{K}$ , the aggregate is formed only in the  
 315 system with 100 THF. The hydrate growth profile in this system (Figure 2(b)) shows  
 316 a slower hydrate growth rate than the system without SDS aggregate, despite having  
 317 more THF. This implies that the SDS micellar aggregate impedes hydrate growth.

318 Though SDS is generally regarded as a kinetic promoter for gas hydrates, several  
 319 studies reported that increasing SDS concentration beyond certain limit compromises

320 the hydrate growth [25, 32]. Experiments showed that the promotion effect of SDS  
321 drops beyond its CMC [31]. Although our observations are obtained at very low SDS  
322 concentrations (0.11mol%), it should, however, be remembered that the time scale  
323 accessible to atomistic MD simulations is on the order of hundreds of nanoseconds,  
324 while the typical exchange rate between surfactants in the bulk and those adsorbed  
325 at interfaces or within micelles is of the order of microseconds. To overcome these  
326 differences in time scale, the few SDS molecules present in our system are initially  
327 placed on the solid-liquid interface (see Figure 1). Nevertheless, the simulation and  
328 the experimental results just summarised are indeed in qualitative agreement.

329 To identify the molecular mechanism responsible for the observations, we hypothesise  
330 a kinetic or thermodynamic effect. In the next paragraphs, we discriminate between  
331 the two possibilities.

### 332 *3.3.1. Hypothesis 1: Kinetic Effects*

333 Lv et al. [32] identified an optimal concentration of surfactant promoters concerning  
334 the growth of methane hydrates. Adding beyond the optimal amount leads to a  
335 decrease in hydrate growth rate and gas storage capacity. They hypothesised that  
336 such phenomena can be ascribed to micelles forming cages that will trap the gas  
337 molecules, hindering mass transfer from the liquid to the hydrate. Stimulated by this  
338 hypothesis, we delved further into understanding micelles' kinetic and thermodynamic  
339 influences on hydrate growth.

340 If the SDS aggregates reduce the kinetics of hydrate growth by removing CO<sub>2</sub> from  
341 the system, it is plausible that the aggregation would lead to a decrease in the con-  
342 centration of CO<sub>2</sub> at the interface, which is the rate-limiting step for hydrate growth  
343 [68]. Since we observe the presence of SDS aggregation in our systems alongside CO<sub>2</sub>,  
344 it is reasonable to assume that these aggregates have an impact on the concentra-  
345 tion of CO<sub>2</sub> at the interface. Hence, the concentration of CO<sub>2</sub> at the hydrate-liquid  
346 interface is analysed at T=284.1K, at which conditions our simulations identify the  
347 largest SDS aggregate. The results are illustrated in Figure S9. We acquired inter-  
348 facial concentrations by identifying the interface using the F4 order parameter and  
349 calculated the concentration within the interfacial region ( $\approx 1\text{nm}$  thick). It can be  
350 inferred from the graph that there are fewer CO<sub>2</sub> molecules at the interface when the  
351 SDS aggregate is present (when THF is present), which agrees with the mass trans-  
352 fer limitation hypothesis by Lv and colleagues [32]. However, the statistical analysis  
353 reveals a different conclusion. We conducted a two-sided t-test between the 100 THF  
354 system (which has the largest SDS aggregate) and the 0 THF system using Python's  
355 scipy library. The p-value obtained is 0.076, which is slightly higher than 0.05, sug-  
356 gesting that the difference in CO<sub>2</sub> concentration at the interface is not statistically  
357 significant. As such, though it is possible that mass transfer limitation could be a  
358 factor in the observed behaviour, this hypothesis cannot be conclusively verified.

### 359 *3.3.2. Hypothesis 2: Thermodynamic Effects*

360 Because the aggregates adsorb and trap a significant amount of THF and CO<sub>2</sub>  
361 molecules, impacts could be exerted on hydrate growth. First, trapping the THF  
362 molecules will reduce their promoting capability. Second, trapping CO<sub>2</sub> will reduce  
363 supersaturation and hence the driving force for hydrate growth.

364 Figure 5 demonstrates the difference in hydrate growth between our systems and the  
365 results reported by Phan et al. [24]. Their work employed an identical simulation

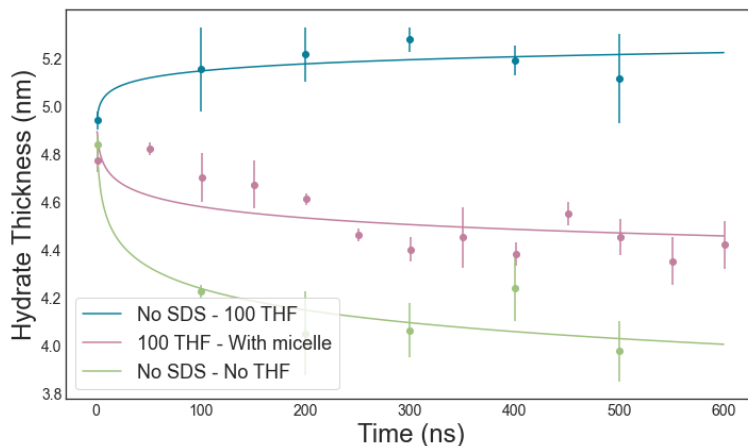


Figure 5: Comparison of hydrate growth removing SDS and  $\text{CO}_2$  within SDS aggregates with literature value with no SDS at  $T=284.1\text{K}$  [24].

366 framework to the one considered here, except no SDS was present. Hence, no aggre-  
 367 gate formed in the systems studied by Phan et al. We obtained the hydrate thickness  
 368 data from two of their systems: one with 100 THF and one without at  $T=284.1\text{K}$ .  
 369 Our THF and  $\text{CO}_2$  concentration and simulation conditions are also identical. Their  
 370 results indicated that THF shifts the equilibrium curve to milder conditions, as the  
 371 hydrates with THF promoters (blue) did not dissociate as much as those with no  
 372 THF (green). Our system with 100 THF and SDS at  $T=284.1\text{K}$  lies in between the  
 373 other two datasets. It is, therefore, apparent that the SDS molecules behave like ther-  
 374 modynamic inhibitors. Figure S8 shows that approximately 50 to 60 THF molecules  
 375 are trapped within the SDS aggregate. As such, Figure 5 can be viewed as the hy-  
 376 drate growth comparison between systems with 100 THF, 50 THF and 0 THF. The  
 377 trend illustrated in Figure 5 agrees well with our simulation results at  $T=269.1\text{K}$  and  
 378  $T=279.1\text{K}$ , where more THF leads to faster growth, as shown in Figure 2. This obser-  
 379 vation supports the hypothesis that SDS aggregate traps THF molecules, removing  
 380 them from the hydrate-liquid interface. This mechanism could only partially explain  
 381 the slower hydrate growth rate obtained for the system with 100 THF compared to  
 382 50 THF at  $T=274.1\text{K}$ , as illustrated in Figure 2 (b). The SDS aggregate in the 100  
 383 THF system only traps 20-30 THF molecules, which means there are still more free  
 384 THF in this system than in the one built to contain 50 THF molecules. This leads  
 385 us to the second thermodynamic hypothesis: that the aggregates reduce the driving  
 386 force by sequestering  $\text{CO}_2$  molecules.

387 To test this possibility, we conducted additional simulations to understand the signif-  
 388 icance of reduced  $\text{CO}_2$  concentration in the bulk liquid on hydrate growth. We used  
 389 the same conditions and configurations as the 100 THF system at  $T=274.1\text{K}$ , but we  
 390 removed the  $\text{CO}_2$  and THF content trapped in the aggregate. To prevent SDS from  
 391 aggregating, we reduced the hydrocarbon tail to only 5 carbon chains so as to increase  
 392 its CMC. Though this would cause a slight deviation in chemical properties from SDS,  
 393 the change in tail length has a limited impact on hydrate growth at a concentration  
 394 above 0.1wt% [69], which is significantly lower than the concentration of SDS used in  
 395 the simulation. The growth profile is presented in Figure 6. It can be deduced from  
 396 the graph in Figure 6 that reducing  $\text{CO}_2$  concentration slows down hydrate growth.  
 397 However, the data sets are within statistical uncertainty from each other, suggesting  
 398 that reducing  $\text{CO}_2$  concentration is not the only mechanism by which the aggregates  
 399 affect hydrates growth.

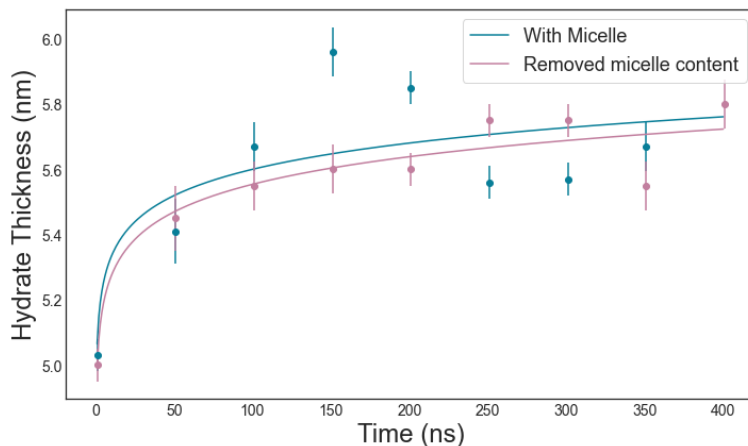


Figure 6: Comparison of hydrate growth removing SDS and  $\text{CO}_2$  within SDS aggregates with literature value with no SDS at  $T=284.1\text{K}$ .

#### 400 4. Experimental Validation

401 The simulation studies discussed above reveal two significant observations. Firstly, it  
 402 is observed that THF decreases the CMC of SDS. Secondly, it is ascertained that the  
 403 occurrence of such SDS micellar aggregates adversely affects the growth of hydrates.  
 404 These conclusions were validated using experiments to authenticate their accuracy  
 405 and robustness.

##### 406 4.1. Interfacial Tension (IFT) Measurements

407 The CMC for each series was determined from the intersection of the concentration-  
 408 dependent section of the ST graph with the horizontal (concentration-independent)  
 409 section of the graph. Below the CMC, ST is linearly dependent on the log of concen-  
 410 tration, whereby an increase in concentration leads to a concurrent decrease in ST.  
 411 Such a relationship occurs because the surfactant adsorbs to the droplet's water-air  
 412 interface and creates a surfactant monolayer. Eventually, at the CMC, the interface  
 413 is saturated with surfactant molecules and the minimum ST for that surfactant sys-  
 414 tem is reached. Above the CMC, additional surfactant adsorption to this interface is  
 415 deterred by the established adsorption layer, and surfactant molecules associate into  
 416 micelles in solution, resulting in little to no further change in ST.

417 The CMC can be interpolated by fitting lines through the concentration-dependent  
 418 and independent regions, respectively and determining the intercept of the two lines.  
 419 In the case of pure SDS, as shown in Figure 7 (a), a CMC value of 7.93 mM was  
 420 extracted, which is consistent with the literature values of 8-8.25 mM at 298K [70, 71].

421 When THF was added to the SDS- $\text{CO}_2$  solutions, as shown in Figure 7 (b), the  
 422 measured CMC decreased by 22.2% to 6.17 mM at 298K and atmospheric pressure.  
 423 The decrease in CMC with both promoters present indicates that the THF and SDS  
 424 interact in solution and that this interaction causes a decrease in the amount of SDS  
 425 that can adsorb to the hydrate surface. Such a significant decrease in CMC also  
 426 reaffirmed the simulation observations.

##### 427 4.2. HP-DSC Results for $\text{CO}_2$ Hydrate Conversion

428 The effect of promoters (THF, SDS, and the combination of both of them) on  $\text{CO}_2$  hy-  
 429 drates properties was inferred by quantities measured during our High-Pressure DSC

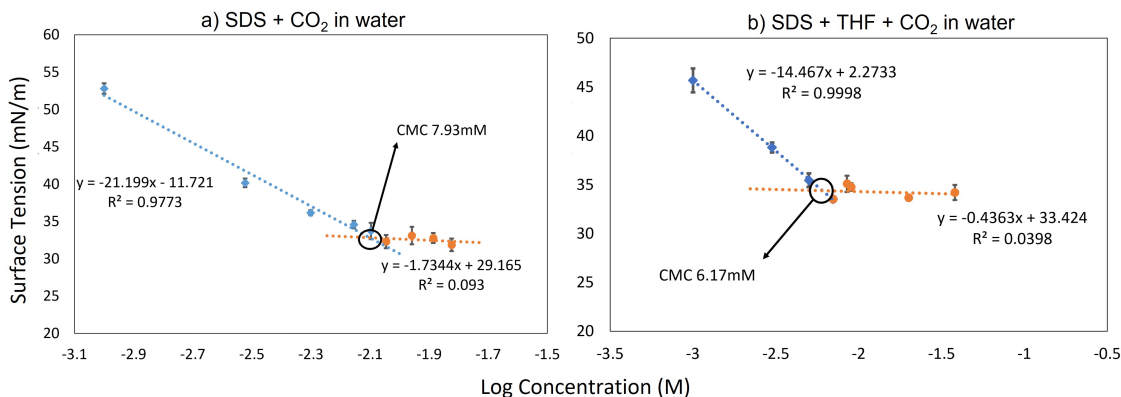


Figure 7: Surface tension vs log concentration for a) pure SDS solutions in CO<sub>2</sub> saturated water from 0.001M to 0.015M SDS with CMC determined as 7.93mM SDS, and b) THF-SDS solutions in CO<sub>2</sub> saturated water from 0.001M to 0.038M SDS with 0.476M THF with CMC determined as 6.17mM SDS. CMC is calculated by equating the fit lines and solving for the point of intersection. Error bars represent 1 standard deviation and are calculated from three repeat experiments per solution across an average of 10 points per repeat.

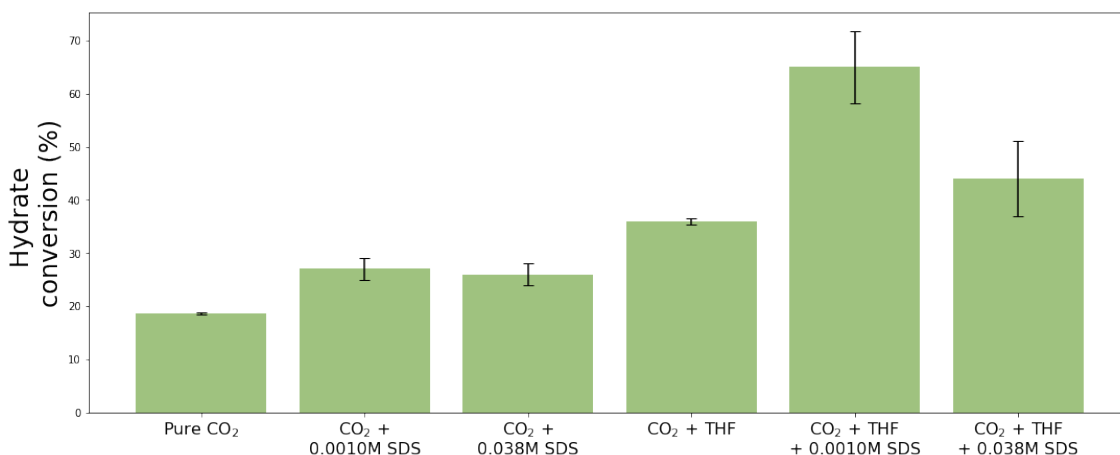


Figure 8: Conversion determined from DSC experiments for CO<sub>2</sub> containing hydrate phases. The experiments were repeated in triplicates to ensure repeatability and reliability of the results.

430 experiments, such as the percentage of CO<sub>2</sub> hydrate conversion, onset temperatures,  
 431 and heat released during CO<sub>2</sub> hydrate formation and dissociation.

432 Pure CO<sub>2</sub> hydrates were first used in our experiments to establish a baseline heat  
 433 release and conversion. The pure CO<sub>2</sub> hydrate experiment produced a single peak  
 434 with an average dissociation onset temperature of  $6.29 \pm 0.11^\circ\text{C}$  and heat of dissoci-  
 435 ation of  $124.36 \pm 1.53 \text{ J/g}$  as produced in Figure S10 (A). This onset temperature is  
 436 similar to what was obtained by Anderson [59], thereby substantiating the accuracy  
 437 and validity of our experimental set-up.

438 Hydrate conversion was compared between CO<sub>2</sub> with SDS at concentrations below  
 439 and above the CMC, respectively. CO<sub>2</sub>-0.001M SDS experiments (below the CMC)  
 440 produced an average dissociation onset temperature of  $6.39 \pm 0.11^\circ\text{C}$ , similar to the  
 441 pure CO<sub>2</sub> system. This implies that SDS did not affect the thermodynamics of the  
 442 system. As seen from Figure S10 (B), only a single peak was obtained from the DSC  
 443 profile, indicating a CO<sub>2</sub> hydrate phase with increased conversion due to the kinetic  
 444 promotion. CO<sub>2</sub>-0.038M SDS (above the CMC) experiments showed a similar DSC  
 445 profile, with a single peak and an average dissociation onset temperature of  $6.38 \pm$



446 0.10°C. The hydrate conversion percentages below and above the CMC are  $27 \pm$   
447  $1.97\%$  and  $26 \pm 2.07\%$ , respectively, with no significant difference as shown in Figure  
448 8. These results indicate that, with SDS alone present in the system, the presence of  
449 SDS micelles does not affect the performance of the kinetic promoter towards sI CO<sub>2</sub>  
450 hydrates. Such observation is consistent with the simulation results shown in Figure  
451 S9, according to which the kinetic hindrance and reduction of concentration driving  
452 force of the micelles are insignificant.

453 Next, 10wt% THF was added to the CO<sub>2</sub> hydrate system to determine the effect of  
454 THF alone. The DSC profile shown in Figure S10 (D) revealed two distinct peaks  
455 corresponding to the formation of THF hydrates and THF-CO<sub>2</sub> hydrates, respectively.  
456 The blue curve plotted in Figure S10 (D) is more likely to be THF hydrates as the  
457 onset temperature is  $3.38 \pm 0.21^\circ\text{C}$ , which is closer to that of a THF hydrate rather  
458 than CO<sub>2</sub> hydrates [37]. The presence of multiple peaks suggests that the addition of  
459 THF can cause the formation of mixed hydrate phases, as shown in other works [60, 72,  
460 73, 74]. The THF-CO<sub>2</sub> hydrates (highlighted in orange in Figure S10 (D)) have a higher  
461 dissociation onset temperature of  $12.63 \pm 0.82^\circ\text{C}$  as compared to CO<sub>2</sub> and CO<sub>2</sub>+SDS  
462 systems shown earlier. The temperature shift conforms to the current understanding  
463 of the thermodynamic promoter role of THF. The broad peak with multiple maxima  
464 indicates that there may be CO<sub>2</sub>-THF hydrates of different THF compositions formed  
465 and dissociated during the experiment, which aligns with previous studies [60, 72].  
466 The conversion for the THF hydrate phase was not calculated as it likely did not  
467 contain CO<sub>2</sub> [60, 72] and thus would not factor into the total CO<sub>2</sub> conversion. As  
468 such, the CO<sub>2</sub> hydrate conversion was computed to be  $36 \pm 0.61\%$ .

469 THF-SDS mixtures were tested to determine the effect of the combined promoter sys-  
470 tem. At both SDS concentrations with THF present, two distinct peaks appeared, in-  
471 dicating hydrates of different compositions may have formed due to THF. The larger,  
472 narrow peaks (highlighted in blue) shifted well above the THF hydrate equilibrium  
473 temperature and towards the CO<sub>2</sub> hydrate equilibrium temperature, indicating that  
474 a pure CO<sub>2</sub> hydrate phase formed in place of the pure THF hydrate phase. The  
475 SDS in the system appears to have encouraged the growth of a pure sI CO<sub>2</sub> hydrate  
476 phase which did not exist when THF alone was present. This is the same conclusion  
477 drawn for methane hydrates by Kumar and colleagues [73]. In both systems, as both  
478 hydrates would contain CO<sub>2</sub>, the conversion was calculated by adding the individual  
479 conversions for the CO<sub>2</sub> and CO<sub>2</sub>-THF hydrate. At 0.001M SDS, below the CMC  
480 (Figure S10 (E)), the total conversion is  $65 \pm 6.76\%$ . At 0.038M SDS above the  
481 CMC (Figure S10 (F)), the amount of CO<sub>2</sub> hydrate formed decreased, indicated by  
482 the lower average heat of dissociation of  $83.84 \pm 46.56 \text{ J/g}$  at  $5.73 \pm 0.09^\circ\text{C}$ , while  
483 the CO<sub>2</sub>-THF hydrate peak remained almost unchanged. The total CO<sub>2</sub> conversion  
484 in this system is computed to be  $44 \pm 7.09\%$ .

485 The comparison of CO<sub>2</sub> conversion in all systems is presented in Figure 8. The  
486 results first reaffirmed the discovery that a combination of THF and SDS is better  
487 when a single promoter is used. However, more importantly, while SDS added in  
488 addition to THF can increase CO<sub>2</sub> hydrate formation, the presence of SDS above  
489 its CMC detrimentally impacts the overall growth and conversion of the hydrate, as  
490 shown from the lower conversion. Below the CMC, the combined application of SDS  
491 and THF drastically increases conversion compared to SDS or THF alone; however,  
492 above the CMC, the SDS and THF detrimentally interact, and the total conversion  
493 decreases.

## 5. Conclusions

### 5.1. Key findings

The synergism vs antagonism between THF and SDS on CO<sub>2</sub> hydrates was investigated using atomistic MD simulations conducted within various temperatures and system compositions. The results show that CO<sub>2</sub> hydrates grow faster with more THF at T=269.1K and T=279.1K at 25.5 bar. Increasing the temperature to 274.1K and beyond, SDS micellar aggregates could appear, likely due to the increasing entropic driving force [65]. Lowering THF concentration can prevent the formation of SDS aggregates, which indicates that THF lowers the critical micelle concentration (CMC) of SDS. This is confirmed by results obtained from IFT experiments. Simulation results reveal that at T = 284.1K with 100 THF molecules, the hydrates dissociated when SDS micelles existed but grew when no SDS was present at the same conditions. The HP-DSC experiments also indicate a decrease in the dissociation temperature when both THF and SDS are present.

### 5.2. Key improvements compared to findings in literature

The synergistic influence of THF and SDS on CO<sub>2</sub> hydrates has been extensively observed through various experimental investigations [15, 28]. It has been observed that the addition of an excessive amount of promoters can have a detrimental effect on their overall performance [29, 75]. The present research findings shed light on the existence of an optimal surfactant concentration that is associated with promoting efficient hydrate growth.

### 5.3. Highlight of hypothesis, new concepts and innovations

The simulation and experiment results indicate that the SDS aggregates behave like thermodynamic inhibitors as they trap THF molecules, essentially removing them and the SDS themselves from the hydrate-liquid interface. Removing THF reduces its thermodynamic stabilisation ability. This phenomenon explains the presence of optimal surfactant concentration related to promoting hydrate growth. CO<sub>2</sub> conversion results obtained from DSC experiments also reinforced this hypothesis. In addition to being consistent with the simulation results, the experiments also show that the CO<sub>2</sub> uptake in hydrates strongly depends on the synergism among the two promoters, with the best results obtained here showing 21% to 46% increase in CO<sub>2</sub> uptake compared to systems without promoters, as well as with system with a sub-optimal composition of the promoters cocktail.

### 5.4. Vision for future work

These results provide insights into understanding the microscopic behaviours of promoters on hydrate growth and how promoters can interact synergistically and/or antagonistically depending on their relative concentrations and the system conditions. Because our results show the possibility of SDS aggregate formation at very low concentrations, future research should aim at uncovering the molecular mechanisms by which SDS acts as a kinetic promoter at low concentrations, below the CMC.

## 6. Acknowledgements

Xinrui Cai would like to express her gratitude towards the A&BK studentship that sponsored this project. Alberto Striolo is grateful to the Asahi Chair in Chemical Engineering at the University of Oklahoma, as well as to the EPSRC grant

538 number EP/T004282/1 for financial support. Matteo Salvalaglio acknowledges fund-  
539 ing from the Crystallization in the Real World EPSRC Programme Grant (Grant  
540 EP/R018820/1) and the EPSRC Frontier Guarantee Grant (EP/X033139/1). Joshua  
541 Worley and Carolyn Koh acknowledge funding from the NSF under the CBET grant  
542 2015201 for experimental work. The authors gratefully acknowledge the Archer2  
543 and UCL myriad teams for providing access to their supercomputing facilities and  
544 technical support, which have greatly advanced this research project.

545 **References**

- 546 [1] B. A. Buffett, “Clathrate Hydrates,” *Annual Review of Earth and Planetary*  
547 *Sciences*, vol. 28, pp. 477–507, may 2000.
- 548 [2] E. D. Sloan Jr. and C. A. Koh, *Clathrate Hydrates of Natural Gases*. CRC Press,  
549 3rd ed., sep 2007.
- 550 [3] E. D. Sloan, “Fundamental principles and applications of natural gas hydrates,”  
551 *Nature*, vol. 426, no. 6964, pp. 353–359, 2003.
- 552 [4] H. P. Veluswamy and P. Linga, “Macroscopic kinetics of hydrate formation of  
553 mixed hydrates of hydrogen/tetrahydrofuran for hydrogen storage,” *Internat-*  
554 *ional Journal of Hydrogen Energy*, vol. 38, pp. 4587–4596, apr 2013.
- 555 [5] H. J. Lee, J. D. Lee, P. Linga, P. Englezos, Y. S. Kim, M. S. Lee, and Y. D. Kim,  
556 “Gas hydrate formation process for pre-combustion capture of carbon dioxide,”  
557 *Energy*, vol. 35, no. 6, pp. 2729–2733, 2010.
- 558 [6] M. Yang, H. Zhou, P. Wang, N. Li, and Y. Song, “Hydrate-based CO<sub>2</sub> capture  
559 from flue gas in constant pressure process with the presence of THF,” *Energy*  
560 *Procedia*, vol. 142, pp. 3939–3943, 2017.
- 561 [7] S. Lee, L. Liang, D. Riestenberg, O. R. West, C. Tsouris, and E. Adams, “CO  
562 2 Hydrate Composite for Ocean Carbon Sequestration,” *Environmental Science*  
563 *& Technology*, vol. 37, pp. 3701–3708, aug 2003.
- 564 [8] T. Saikia and A. Sultan, “Hydrate-based CO<sub>2</sub> separation,” in *Emerging Carbon*  
565 *Capture Technologies*, ch. 7, pp. 193–237, Elsevier Inc., 2022.
- 566 [9] P. W. Wang, D. T. Wu, and S. T. Lin, “Promotion mechanism for the growth of  
567 CO<sub>2</sub>hydrate with urea using molecular dynamics simulations,” *Chemical Com-*  
568 *munications*, vol. 57, no. 43, pp. 5330–5333, 2021.
- 569 [10] H. Dashti, L. Zhehao Yew, and X. Lou, “Recent advances in gas hydrate-based  
570 CO<sub>2</sub> capture,” *Journal of Natural Gas Science and Engineering*, vol. 23, pp. 195–  
571 207, 2015.
- 572 [11] H. Hoteit, M. Fahs, and M. R. Soltanian, “Assessment of CO<sub>2</sub> Injectivity During  
573 Sequestration in Depleted Gas Reservoirs,” *Geosciences*, vol. 9, p. 199, may 2019.
- 574 [12] J.-H. Sa, B. R. Lee, D.-H. Park, K. Han, H. D. Chun, and K.-H. Lee, “Amino  
575 Acids as Natural Inhibitors for Hydrate Formation in CO<sub>2</sub> Sequestration,” *En-*  
576 *vironmental Science Technology*, vol. 45, pp. 5885–5891, jul 2011.
- 577 [13] A. A. Majid, J. Worley, and C. A. Koh, “Thermodynamic and Kinetic Promoters  
578 for Gas Hydrate Technological Applications,” *Energy and Fuels*, vol. 35, no. 23,  
579 pp. 19288–19301, 2021.
- 580 [14] Y. Li, A. M. Gambelli, F. Rossi, and S. Mei, “Effect of promoters on CO<sub>2</sub>  
581 hydrate formation: thermodynamic assessment and microscale Raman spec-
- 582 troscopy/hydrate crystal morphology characterization analysis,” *Fluid Phase*  
583 *Equilibria*, vol. 550, p. 113218, 2021.

- 584 [15] H. P. Veluswamy, K. P. Premasinghe, and P. Linga, "CO<sub>2</sub> Hydrates - Effect of  
585 Additives and Operating Conditions on the Morphology and Hydrate Growth,"  
586 *Energy Procedia*, vol. 105, pp. 5048–5054, 2017.
- 587 [16] N. Xu, Y. Liu, Z. Cheng, S. Wang, L. Jiang, and Y. Song, "Morphology-Based  
588 Kinetic Study of the Formation of Carbon Dioxide Hydrates with Promoters,"  
589 *Energy & Fuels*, vol. 34, pp. 7307–7315, jun 2020.
- 590 [17] O. Salako, C. Lo, J. Zhang, A. Couzis, P. Somasundaran, and J. Lee, "Adsorption  
591 of sodium dodecyl sulfate onto clathrate hydrates in the presence of salt," *Journal*  
592 *of Colloid and Interface Science*, vol. 386, pp. 333–337, nov 2012.
- 593 [18] J. S. Zhang, S. Lee, and J. W. Lee, "Kinetics of Methane Hydrate Formation from  
594 SDS Solution," *Industrial Engineering Chemistry Research*, vol. 46, pp. 6353–  
595 6359, sep 2007.
- 596 [19] A. Kumar, G. Bhattacharjee, B. D. Kulkarni, and R. Kumar, "Role of Surfac-  
597 tants in Promoting Gas Hydrate Formation," *Industrial Engineering Chemistry*  
598 *Research*, vol. 54, pp. 12217–12232, dec 2015.
- 599 [20] J. Yoslim, P. Linga, and P. Englezos, "Enhanced growth of methane–propane  
600 clathrate hydrate crystals with sodium dodecyl sulfate, sodium tetradecyl sulfate,  
601 and sodium hexadecyl sulfate surfactants," *Journal of Crystal Growth*, vol. 313,  
602 pp. 68–80, dec 2010.
- 603 [21] C. Lo, J. Zhang, P. Somasundaran, and J. W. Lee, "Investigations of surfactant  
604 effects on gas hydrate formation via infrared spectroscopy," *Journal of Colloid*  
605 *and Interface Science*, vol. 376, pp. 173–176, jun 2012.
- 606 [22] H. Liang, D. Guan, Y. Liu, L. Zhang, J. Zhao, L. Yang, and Y. Song, "Kinetic  
607 process of upward gas hydrate growth and water migration on the solid surface,"  
608 *Journal of Colloid and Interface Science*, vol. 626, pp. 1003–1014, nov 2022.
- 609 [23] S. P. Kang, H. Lee, C. S. Lee, and W. M. Sung, "Hydrate phase equilibria  
610 of the guest mixtures containing CO<sub>2</sub>, N<sub>2</sub> and tetrahydrofuran," *Fluid Phase*  
611 *Equilibria*, vol. 185, no. 1-2, pp. 101–109, 2001.
- 612 [24] A. Phan, H. Schlösser, and A. Striolo, "Molecular mechanisms by which tetrahy-  
613 drofuran affects CO<sub>2</sub> hydrate Growth: Implications for carbon storage," *Chem-*  
614 *ical Engineering Journal*, vol. 418, no. December 2020, pp. 34–37, 2021.
- 615 [25] L. Liu, Y. Yao, X. Zhou, Y. Zhang, and D. Liang, "Improved formation kinetics  
616 of carbon dioxide hydrate in brine induced by sodium dodecyl sulfate," *Energies*,  
617 vol. 14, no. 8, 2021.
- 618 [26] D. L. Zhong, S. Y. He, D. J. Sun, and C. Yang, "Comparison of methane hydrate  
619 formation in stirred reactor and porous media in the presence of SDS," *Energy*  
620 *Procedia*, vol. 61, pp. 1573–1576, 2014.
- 621 [27] N. S. Molokitina, A. N. Nesterov, L. S. Podenko, and A. M. Reshetnikov, "Car-  
622 bon dioxide hydrate formation with SDS: Further insights into mechanism of gas  
623 hydrate growth in the presence of surfactant," *Fuel*, vol. 235, no. March 2018,  
624 pp. 1400–1411, 2019.

- 625 [28] J. P. Torr , M. Ricaurte, C. Dicharry, and D. Broseta, “CO 2 enclathration in  
626 the presence of water-soluble hydrate promoters: Hydrate phase equilibria and  
627 kinetic studies in quiescent conditions,” *Chemical Engineering Science*, vol. 82,  
628 pp. 1–13, 2012.
- 629 [29] H. Wang, Q. Wu, and B. Zhang, “Influence of THF and THF/SDS on the Kinet-  
630 ics of CO2 Hydrate Formation Under Stirring,” *Frontiers in Energy Research*,  
631 vol. 9, feb 2021.
- 632 [30] J. S. Zhang, C. Lo, P. Somasundaran, and J. W. Lee, “Competitive adsorption  
633 between SDS and carbonate on tetrahydrofuran hydrates,” *Journal of Colloid  
634 and Interface Science*, vol. 341, pp. 286–288, jan 2010.
- 635 [31] J. Tang, D. Zeng, C. Wang, Y. Chen, L. He, and N. Cai, “Study on the influ-  
636 ence of SDS and THF on hydrate-based gas separation performance,” *Chemical  
637 Engineering Research and Design*, vol. 91, pp. 1777–1782, sep 2013.
- 638 [32] X. Lv, D. Lu, Y. Liu, S. Zhou, J. Zuo, H. Jin, B. Shi, and E. Li, “Study on  
639 methane hydrate formation in gas-water systems with a new compound pro-  
640 moter,” *RSC Advances*, vol. 9, no. 57, pp. 33506–33518, 2019.
- 641 [33] A. Demurov, R. Radhakrishnan, and B. L. Trout, “Computations of diffusivities  
642 in ice and CO2 clathrate hydrates via molecular dynamics and Monte Carlo  
643 simulations,” *The Journal of Chemical Physics*, vol. 116, pp. 702–709, jan 2002.
- 644 [34] N. I. Papadimitriou, I. N. Tsimpanogiannis, I. G. Economou, and A. K. Stubos,  
645 “Monte Carlo simulations of the separation of a binary gas mixture (CH 4 +  
646 CO 2 ) using hydrates,” *Physical Chemistry Chemical Physics*, vol. 20, no. 44,  
647 pp. 28026–28038, 2018.
- 648 [35] Y. J. Lee, T. Kawamura, Y. Yamamoto, and J. H. Yoon, “Phase equilibrium  
649 studies of tetrahydrofuran (THF) + CH4, THF + CO2, CH4 + CO2, and THF  
650 + CO2 + CH4 hydrates,” *Journal of Chemical and Engineering Data*, vol. 57,  
651 no. 12, pp. 3543–3548, 2012.
- 652 [36] F. Takeuchi, M. Hiratsuka, R. Ohmura, S. Alavi, A. K. Sum, and K. Yasuoka,  
653 “Water proton configurations in structures I, II, and H clathrate hydrate unit  
654 cells,” *Journal of Chemical Physics*, vol. 138, no. 12, 2013.
- 655 [37] A. Delahaye, L. Fournaison, S. Marinhas, I. Chatti, J.-P. Petitet, D. Dalmaz-  
656 zone, and W. F rst, “Effect of THF on Equilibrium Pressure and Dissociation  
657 Enthalpy of CO 2 Hydrates Applied to Secondary Refrigeration,” *Industrial En-  
658 gineering Chemistry Research*, vol. 45, pp. 391–397, jan 2006.
- 659 [38] L. Jensen, K. Thomsen, N. von Solms, S. Wierzchowski, M. R. Walsh, C. A. Koh,  
660 E. D. Sloan, D. T. Wu, and A. K. Sum, “Calculation of Liquid Water-Hydrate-  
661 Methane Vapor Phase Equilibria from Molecular Simulations,” *The Journal of  
662 Physical Chemistry B*, vol. 114, pp. 5775–5782, may 2010.
- 663 [39] J. M. M guez, M. M. Conde, J. P. Torr , F. J. Blas, M. M. Pi neiro, and C. Vega,  
664 “Molecular dynamics simulation of CO2 hydrates: Prediction of three phase  
665 coexistence line,” *Journal of Chemical Physics*, vol. 142, no. 12, 2015.

- 666 [40] M. M. Conde and C. Vega, "Determining the three-phase coexistence line  
667 in methane hydrates using computer simulations," *The Journal of Chemical*  
668 *Physics*, vol. 133, p. 064507, aug 2010.
- 669 [41] J. G. Harris and K. H. Yung, "Carbon Dioxide's Liquid-Vapor Coexistence Curve  
670 And Critical Properties as Predicted by a Simple Molecular Model," *The Journal*  
671 *of Physical Chemistry*, vol. 99, pp. 12021–12024, aug 1995.
- 672 [42] Y. T. Tung, L. J. Chen, Y. P. Chen, and S. T. Lin, "Growth of structure i car-  
673 bon dioxide hydrate from molecular dynamics simulations," *Journal of Physical*  
674 *Chemistry C*, vol. 115, no. 15, pp. 7504–7515, 2011.
- 675 [43] P. Procacci, "PrimaDORAC: A Free Web Interface for the Assignment of Par-  
676 tial Charges, Chemical Topology, and Bonded Parameters in Organic or Drug  
677 Molecules," *Journal of Chemical Information and Modeling*, vol. 57, pp. 1240–  
678 1245, jun 2017.
- 679 [44] H. Dominguez and M. L. Berkowitz, "Computer Simulations of Sodium Dodecyl  
680 Sulfate at Liquid/Liquid and Liquid/Vapor Interfaces," *The Journal of Physical*  
681 *Chemistry B*, vol. 104, pp. 5302–5308, jun 2000.
- 682 [45] V. K. Michalis, I. N. Tsimpanogiannis, A. K. Stubos, and I. G. Economou,  
683 "Direct phase coexistence molecular dynamics study of the phase equilibria of  
684 the ternary methane-carbon dioxide-water hydrate system," *Physical Chemistry*  
685 *Chemical Physics*, vol. 18, no. 34, pp. 23538–23548, 2016.
- 686 [46] H. Berendsen, D. van der Spoel, and R. van Drunen, "GROMACS: A message-  
687 passing parallel molecular dynamics implementation," *Computer Physics Com-*  
688 *munications*, vol. 91, pp. 43–56, sep 1995.
- 689 [47] H. J. C. Berendsen, J. P. M. Postma, W. F. van Gunsteren, A. DiNola, and J. R.  
690 Haak, "Molecular dynamics with coupling to an external bath," *The Journal of*  
691 *Chemical Physics*, vol. 81, pp. 3684–3690, oct 1984.
- 692 [48] D. J. Evans and B. L. Holian, "The Nose–Hoover thermostat," *The Journal of*  
693 *Chemical Physics*, vol. 83, pp. 4069–4074, oct 1985.
- 694 [49] M. Parrinello and A. Rahman, "Crystal Structure and Pair Potentials: A  
695 Molecular-Dynamics Study," *Physical Review Letters*, vol. 45, pp. 1196–1199,  
696 oct 1980.
- 697 [50] T. Yagasaki, M. Matsumoto, and H. Tanaka, "Mechanism of Slow Crystal  
698 Growth of Tetrahydrofuran Clathrate Hydrate," *The Journal of Physical Chem-*  
699 *istry C*, vol. 120, pp. 3305–3313, feb 2016.
- 700 [51] Y. Zhang, S. E. Feller, B. R. Brooks, and R. W. Pastor, "Computer simulation of  
701 liquid/liquid interfaces. I. Theory and application to octane/water," *The Journal*  
702 *of Chemical Physics*, vol. 103, pp. 10252–10266, dec 1995.
- 703 [52] S. Adisasmito, R. J. Frank, and E. D. Sloan, "Hydrates of carbon dioxide and  
704 methane mixtures," *Journal of Chemical & Engineering Data*, vol. 36, pp. 68–71,  
705 jan 1991.

- 706 [53] P. Rodger, T. Forester, and W. Smith, "Simulations of the methane hy-  
707 drate/methane gas interface near hydrate forming conditions conditions," *Fluid*  
708 *Phase Equilibria*, vol. 116, pp. 326–332, mar 1996.
- 709 [54] T. Bui, F. Sicard, D. Monteiro, Q. Lan, M. Ceglio, C. Burrell, and A. Striolo,  
710 "Antiagglomerants Affect Gas Hydrate Growth," *Journal of Physical Chemistry*  
711 *Letters*, vol. 9, no. 12, pp. 3491–3496, 2018.
- 712 [55] K. W. Hall, S. Carpendale, and P. G. Kusalik, "Evidence from mixed hydrate  
713 nucleation for a funnel model of crystallization," 2016.
- 714 [56] G. A. Tribello, F. Giberti, G. C. Sosso, M. Salvalaglio, and M. Parrinello, "Ana-  
715 lyzing and driving cluster formation in atomistic simulations," *Journal of chem-*  
716 *ical theory and computation*, vol. 13, no. 3, pp. 1317–1327, 2017.
- 717 [57] L. Kollias, R. Rousseau, V.-A. Glezakou, and M. Salvalaglio, "Understanding  
718 metal–organic framework nucleation from a solution with evolving graphs," *Jour-*  
719 *nal of the American Chemical Society*, vol. 144, no. 25, pp. 11099–11109, 2022.
- 720 [58] S. Denning, A. A. Majid, J. M. Lucero, J. M. Crawford, M. A. Carreon, and  
721 C. A. Koh, "Metal–Organic Framework HKUST-1 Promotes Methane Hydrate  
722 Formation for Improved Gas Storage Capacity," *ACS Applied Materials Inter-*  
723 *faces*, vol. 12, pp. 53510–53518, nov 2020.
- 724 [59] G. K. Anderson, "Enthalpy of dissociation and hydration number of carbon  
725 dioxide hydrate from the Clapeyron equation," *The Journal of Chemical Ther-*  
726 *modynamics*, vol. 35, pp. 1171–1183, jul 2003.
- 727 [60] M. C. Martínez, D. Dalmazzone, W. Fürst, A. Delahaye, and L. Fournaison,  
728 "Thermodynamic properties of THF + CO<sub>2</sub> hydrates in relation with refrigera-  
729 tion applications," *AIChE Journal*, vol. 54, pp. 1088–1095, apr 2008.
- 730 [61] Q. Sun and Y. T. Kang, "Review on CO<sub>2</sub> hydrate formation/dissociation and  
731 its cold energy application," *Renewable and Sustainable Energy Reviews*, vol. 62,  
732 pp. 478–494, 2016.
- 733 [62] P. Zhang, Q. Wu, C. Mu, and X. Chen, "Nucleation Mechanisms of CO<sub>2</sub> Hydrate  
734 Reflected by Gas Solubility," *Scientific Reports*, vol. 8, no. 1, pp. 1–12, 2018.
- 735 [63] L. S. Chu, D. T. Wu, and S. T. Lin, "Theory and Kinetic Monte Carlo Simulation  
736 of Guest Molecule Transport in sI Clathrate Hydrates Based on Cage Hopping,"  
737 *Journal of Physical Chemistry C*, vol. 123, no. 17, pp. 11233–11243, 2019.
- 738 [64] M. D. Smith, B. Mostofian, L. Petridis, X. Cheng, and J. C. Smith, "Molecular  
739 Driving Forces behind the Tetrahydrofuran-Water Miscibility Gap," *Journal of*  
740 *Physical Chemistry B*, vol. 120, no. 4, pp. 740–747, 2016.
- 741 [65] L. Maibaum, A. R. Dinner, and D. Chandler, "Micelle Formation and the Hy-  
742 drophobic Effect," *The Journal of Physical Chemistry B*, vol. 108, pp. 6778–6781,  
743 may 2004.
- 744 [66] M. Manabe and M. Koda, "The Effect of Poly(oxyethylene) Alkyl Ethers, Alka-  
745 nediols, and Alkanols on the Critical Micelle Concentration of Sodium Dodecyl  
746 Sulfate," *Bulletin of the Chemical Society of Japan*, vol. 51, no. 6, pp. 1599–1601,  
747 1978.



- 748 [67] N. Riesco and J. Trusler, “Novel optical flow cell for measurements of fluid phase  
749 behaviour,” *Fluid Phase Equilibria*, vol. 228-229, pp. 233–238, feb 2005.
- 750 [68] A. Phan, M. Stamatakis, C. A. Koh, and A. Striolo, “Microscopic insights on  
751 clathrate hydrate growth from non-equilibrium molecular dynamics simulations,”  
752 *Journal of Colloid and Interface Science*, vol. 649, pp. 185–193, nov 2023.
- 753 [69] T. Daimaru, A. Yamasaki, and Y. Yanagisawa, “Effect of surfactant carbon  
754 chain length on hydrate formation kinetics,” *Journal of Petroleum Science and  
755 Engineering*, vol. 56, pp. 89–96, mar 2007.
- 756 [70] T. P. Niraula, A. Bhattarai, and S. K. Chatterjee, “Critical micelle concentration  
757 of sodium dodecyl sulphate in pure water and in methanol-water mixed solvent  
758 media in presence and absence of KCl by surface tension and viscosity methods,”  
759 *BIBECHANA*, vol. 11, pp. 103–112, may 2014.
- 760 [71] Y. Moroi, K. Motomura, and R. Matuura, “The critical micelle concentration  
761 of sodium dodecyl sulfate-bivalent metal dodecyl sulfate mixtures in aqueous  
762 solutions,” *Journal of Colloid and Interface Science*, vol. 46, pp. 111–117, jan  
763 1974.
- 764 [72] Q. Sun, S. Kim, and Y. T. Kang, “Study on dissociation characteristics of CO<sub>2</sub>  
765 hydrate with THF for cooling application,” *Applied Energy*, vol. 190, pp. 249–  
766 256, mar 2017.
- 767 [73] A. Kumar, R. Kumar, and P. Linga, “Sodium Dodecyl Sulfate Preferentially Pro-  
768 motes Enclathration of Methane in Mixed Methane-Tetrahydrofuran Hydrates,”  
769 *iScience*, vol. 14, pp. 136–146, apr 2019.
- 770 [74] A. Kumar, N. Daraboina, R. Kumar, and P. Linga, “Experimental Investigation  
771 To Elucidate Why Tetrahydrofuran Rapidly Promotes Methane Hydrate Forma-  
772 tion Kinetics: Applicable to Energy Storage,” *The Journal of Physical Chemistry  
773 C*, vol. 120, pp. 29062–29068, dec 2016.
- 774 [75] D. Mech, P. Gupta, and J. S. Sangwai, “Kinetics of methane hydrate formation  
775 in an aqueous solution of thermodynamic promoters (THF and TBAB) with and  
776 without kinetic promoter (SDS),” *Journal of Natural Gas Science and Engineer-  
777 ing*, vol. 35, pp. 1519–1534, sep 2016.